AGU PUBLICATIONS

JGR

Journal of Geophysical Research: Atmospheres

RESEARCH ARTICLE
10.1002/2015JD023712

Key Points:
- Autonomous setup measuring sea ice-albedo and mass balance deployed in high Arctic in 2012 and 2013
- Air and surface conditions and their influences on ice-ocean system examined with different data
- Earlier melt onset in 2012 was an important factor driving the more dramatic melt in that year

Supporting Information:
- Figure S1

Correspondence to:
C. Wang,
caixin.wang@npolar.no

Citation:
Wang, C., M. A. Granskog, S. R. Hudson, S. Gerland, A. K. Pavlov, D. K. Perovich, and M. Nicolaus (2016), Atmospheric conditions in the central Arctic Ocean through the melt seasons of 2012 and 2013: Impact on surface conditions and solar energy deposition into the ice-ocean system, *J. Geophys. Res. Atmos.*, *121*, 1043–1058, doi:10.1002/2015JD023712.

Received 27 MAY 2015
Accepted 21 DEC 2015
Accepted article online 29 DEC 2015
Published online 5 FEB 2016

Atmospheric conditions in the central Arctic Ocean through the melt seasons of 2012 and 2013: Impact on surface conditions and solar energy deposition into the ice-ocean system

Caixin Wang[1], Mats A. Granskog[1], Stephen R. Hudson[1], Sebastian Gerland[1], Alexey K. Pavlov[1], Donald K. Perovich[2], and Marcel Nicolaus[3]

[1]Norwegian Polar Institute, Fram Centre, Tromsø, Norway, [2]Cold Regions Research and Engineering Laboratory, Hanover, New Hampshire, USA, [3]Alfred-Wegener-Institut, Helmholtz-Zentrum für Polar- und Meeresforschung, Bremerhaven, Germany

Abstract Spectral Radiation Buoys and ice mass balance buoys were deployed on first-year ice near the North Pole in April 2012 and 2013, collecting in-band (350–800 nm) solar radiation and ice and snow mass balance data over the complete summer melt seasons. With complementary European ERA-Interim reanalysis, National Centers for Environmental Prediction (NCEP) Climate forecast system version 2 (CFSv2) analysis and satellite passive microwave data, we examine the evolution of atmospheric and surface melt conditions in the two differing melt seasons. Prevailing atmospheric conditions contributed to a longer and more continuous melt season in summer 2012 than in 2013, which was corroborated by in situ observations. ERA-Interim reanalysis data showed that longwave radiation likely played a key role in delaying the snowmelt onset in 2013. The earlier melt onset in 2012 reduced the albedo, providing a positive ice-albedo feedback at a time when solar insolation was high. Due to earlier melt onset and later freeze-up in 2012, more solar heat was deposited into the ice-ocean system than in 2013. Summer 2013 was characterized by later melt onset, intermittent freezing events and an earlier fall freeze-up, resulting in considerably fewer effective days of surface melt and a higher average albedo. Calculations for idealized seasonal albedo evolution show that moving the melt onset just 1 week earlier in mid-June increases the total absorbed solar radiation by nearly 14% for the summer season. Therefore, the earlier melt onset may have been one of the most important factors driving the more dramatic melt season in 2012 than 2013, though atmospheric circulation patterns, e.g., cyclone in early August 2012, likely contributed as well.

1. Introduction

In recent years, Arctic sea ice has decreased in extent [*Comiso et al.*, 2008] and in thickness [*Haas et al.*, 2008; *Kwok and Rothrock*, 2009; *Hansen et al.*, 2013; *Laxon et al.*, 2013; *Renner et al.*, 2014] and shifted toward a younger ice pack [*Nghiem et al.*, 2007; *Maslanik et al.*, 2007, 2011]. Thus, first-year ice (FYI) has become the dominant ice type, rather than multiyear ice (MYI) [*Maslanik et al.*, 2011]. The observed decline of Arctic sea ice has been attributed to various interrelated causes, including a general overall warming trend [*Steel et al.*, 2008; *Polyakov et al.*, 2010], increased solar heat input to the ocean [*Perovich et al.*, 2007, 2008, 2011a, 2011b; *Nicolaus et al.*, 2012; *Hudson et al.*, 2013], and lengthening of the melt season [*Smith*, 1998; *Markus et al.*, 2009; *Wang et al.*, 2013; *Stroeve et al.*, 2014]. The importance of solar heating to the sea ice mass balance in the central Arctic (north of 80°N) has recently been demonstrated through observations of considerable surface and bottom ice melt in recent years [*Perovich et al.*, 2014a], including summer 2012 [*Wang et al.*, 2014].

There are few long-term (seasonal) observations of the solar radiation partitioning between that which is reflected to the atmosphere and that absorbed in the ice-ocean system, especially in the new thinner Arctic sea ice regime. Arctic MYI was monitored during the 1997–1998 Surface Heat Budget of the Arctic Ocean (SHEBA) experiment [*Perovich et al.*, 2002; *Light et al.*, 2008] and during the Tara drift in the International Polar Year 2007–2008 [*Nicolaus et al.*, 2010a]. More frequent observations have been made on Arctic landfast FYI [*Perovich and Polashenski*, 2012] but at much lower latitudes than the central Arctic Basin. *Perovich et al.* [2007] examined the importance of the timing of melt onset for solar heat input to the ice-ocean system relative to the timing of the freeze-up using albedo observations made on MYI during SHEBA and showed that 1 day

earlier snowmelt onset on top of MYI could result in an additional 0.03 m summer ice melt. On thinner ice with lower albedo this effect could be larger.

The shift to thinner FYI changes solar radiation partitioning and results in lower albedo and larger solar heat input into the ice-ocean system, especially to the ocean below, compared to MYI [*Nicolaus et al*., 2012; *Perovich and Polashenski*, 2012; *Hudson et al*., 2013; *Arndt and Nicolaus*, 2014; *Light et al*., 2015a]. It also impacts the Arctic ecosystem [*Arrigo et al*., 2012; *Brown and Arrigo*, 2013] and increases the potential for human activities in the central Arctic Basin. However, few detailed studies have been carried out to date to examine the partitioning of solar radiation in a FYI system in the central Arctic Basin. *Nicolaus et al*. [2012] and *Hudson et al*. [2013] presented some observations, but only from late summer. Recently, seasonal solar radiation observations were carried out autonomously on FYI in the central Arctic during spring to summer 2012 [*Wang et al*., 2014]. Here we present similar observations from the 2013 season, and we compare the data from the two years.

Conditions in the Arctic Ocean were very different in the two summers of 2012 and 2013 [*Jeffries et al*., 2013]. Since the start of the modern satellite era (from 1979), 2012 was the year with the lowest minimum summer ice extent (3.41×10^6 km^2, only 55% of the 1981–2010 average) [*Jeffries and Richter-Menge*, 2013; *Perovich et al*., 2014b], while 2013 had the seventh lowest minimum extent (5.10×10^6 km^2) [*Perovich et al*., 2013]. Sea ice loss between maximum extent in March and minimum extent in September 2013 was 9.69×10^6 km^2, the smallest seasonal decline since 2006 [*Perovich et al*., 2013]. There was substantial ice bottom and surface melt in 2012 in the central Arctic but considerably less melt in 2013 [*Perovich et al*., 2014a]. Sea level pressure patterns were also quite different [*Overland et al*., 2012, 2013], and thus, the ice dynamics and atmospheric conditions likely differed between the two melt seasons.

Shortwave radiation and snow and ice mass balance of FYI were observed in the central Arctic using autonomous buoys from spring to fall 2012 [see *Wang et al*., 2014] and 2013. We examine the differences in surface and atmospheric conditions in the two melt seasons and investigate how the conditions affected the solar heat input in the ice-ocean system and thus sea ice melt in the central Arctic.

2. Data Collection

The shortwave radiation observations were carried out with an autonomous Spectral Radiation Buoy (SRB). The SRB includes three Satlantic HyperOCR spectroradiometers with two in the air (down and upward looking), and one in the water below the ice (upward looking toward the ice bottom) to measure the in-band (wavelength range between 350 and 800 nm) incident, reflected and transmitted solar radiation above and below the sea ice; for details, see *Wang et al*. [2014]. SRBs were deployed near the North Pole at the temporary Russian ice camp Barneo in April 2012 [*Wang et al*., 2014] and 2013 (Figure 1), colocated with Ice Mass Balance (IMB) buoys [*Richter-Menge et al*., 2006]. The initial positions of the ice floes were in the Amundsen Basin, approximately 55 km from the North Pole, slightly farther west in 2013 than in 2012 (Figure 1). Thereafter, in both years, they drifted southward toward Fram Strait. The southward progression of the SRBs occurred at a very similar rate in the two years until the end of July, but afterward, the SRB moved more rapidly southward in 2012 (Table 1), reaching 79°N in 2012 and 83°N in 2013 by early October (Figure 1). The drift trajectory of the ice floe was substantially shorter in 2013 (1305 km) than in 2012 (2235 km) during the whole drift period (mid-April to early October).

IMBs (numbers 2012C and 2013E [*Perovich et al*., 2014c]) were installed a few meters from the SRBs and automatically measured distances to the snow/ice surface and ice bottom, atmospheric pressure, and temperature of the air, snow, ice, and the upper ocean. Knowing initial snow depth and ice thickness, changes in the distances to the snow/ice surface and to the ice bottom are used to estimate snow evolution and sea ice surface and bottom melting, which links to the energy balance of sea ice. Temperatures of snow, ice, and the upper ocean were measured every 0.1 m with an accuracy of 0.1°C, using a 4.5 m long thermistor string. The atmospheric temperature sensor was shielded but unventilated, which could lead to a warm bias at times due to reflected radiation, but the persistent near-zero summer temperatures suggest that this was not a significant problem.

In both years, two webcams were installed near the SRB site, pointing in opposite directions, as part of the North Pole Environmental Observatory (NPEO), University of Washington, USA. The webcams provide

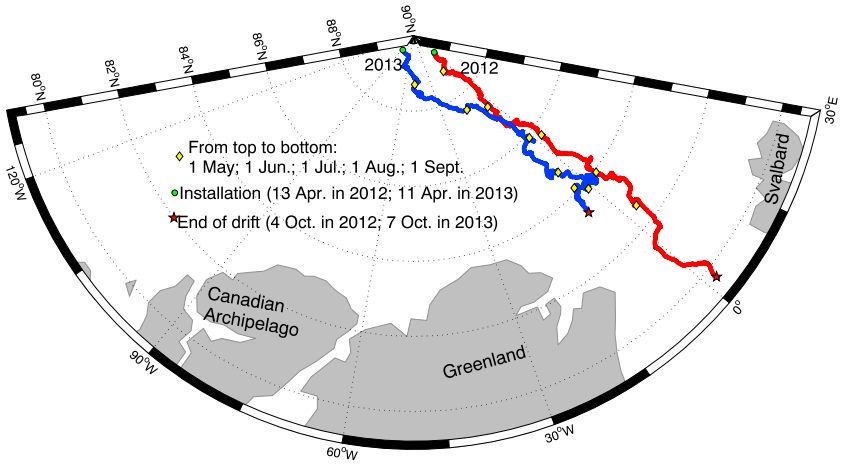

Figure 1. Trajectories of the ice floes carrying IMBs and SRBs in 2012 (red line) and 2013 (blue line).

additional information about the surface evolution, weather, and sky conditions [cf. *Wang et al*., 2014]. Surface melt onset was estimated from the satellite passive microwave data using the difference between brightness temperature (TbD) of the 19 V and 37 V channels on Defense Meteorological Satellite Program Special Sensor Microwave Imager/Sounder (SSMIS) [*Maslanik and Stroeve*, 1990, 2014; *Markus et al*., 2009; *Wang et al*., 2013; *Anderson et al*., 2014; *Bliss and Anderson*, 2014]. When TbD is less than zero, the surface is assumed to be melting [*Wang et al*., 2013]. To account for differences in open water fractions, the TbD in this study is adjusted using the ice concentration [*Cavalieri et al*., 1990, 2014] as in *Markus et al*. [2009].

The European ERA-Interim reanalysis data and NCEP-CFSv2 analysis data are used to investigate the surface energy budget and atmospheric conditions in 2012 and 2013. The ERA-Interim reanalysis data are the latest global atmospheric reanalysis produced by the ECMWF (European Centre for Medium-Range Weather Forecast), available from 1989 onward [*Dee et al*., 2011]. The ERA-Interim reanalysis routines provide major improvements compared with ERA-40, e.g., better vertical consistency of the air temperature in the Arctic region [*Dee and Uppala*, 2009], and an improved representation of the hydrological cycle. The CFSv2 is the second version of the NCEP Climate Forecast System made operational at NCEP in March 2011 [*Saha et al*., 2014]. It is a full-coupled model representing the interaction between the Earth's oceans, land, and atmosphere. It has upgrades to nearly all aspects of the data assimilation and forecast model components of the system. It includes CFSv2 Reanalysis data sets over 1979–2010, and analysis data over 2011–present. The data used in this study are the mean sea level pressure (SLP), 2 m air temperature, 10 m U and V wind components, and surface radiative and turbulent energy fluxes from the ERA-Interim reanalysis data and CFSv2 analysis data. The radiative and turbulent fluxes include net shortwave (netSW) and net longwave (netLW) radiation, and latent (L) and sensible (H) heat fluxes, which have previously been validated over the central Arctic Ocean [e.g., *Jakobson et al*., 2012] and used to explain the interannual and spatial variations in snowmelt onset in the central Arctic [*Maksimovich and Vihma*, 2012]. The net surface heat flux (netF) is the sum of netSW, netLW, and L and H fluxes. Positive values represent heat flux from the atmosphere to the surface.

Table 1. Summary of IMB and SRB Locations and Surface Conditions During Observations

		Date (dd/mm)						Snow				
		1/5	1/6	1/7	1/8	1/9	1/10		Date (dd/mm)			
Year	Operation Period	Latitude (°N)						Depth[a]	Melt Onset	Fully Melted	Refreeze Date (dd/mm)	Melt Duration Days
2012	13/04–7/10	88.8	87.3	85.7	83.9	82.6	80.1	42	10/6	14/07	19/08	71
2013	11/04–4/10	88.7	87.6	85.9	84.7	83.8	84.1	5	20/6	23/07	03/08	45

[a]Measured in situ mean snow depth (cm) in mid-April at deployment.

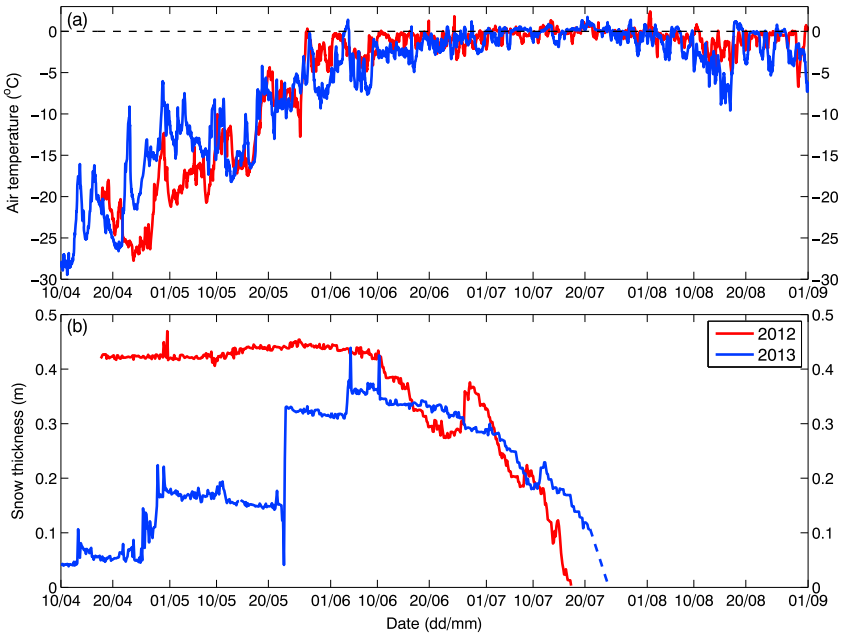

Figure 2. (a) Air temperature and (b) snow thickness at the SRB/IMB sites in 2012 (red line) and in 2013 (blue line). Snow depth data were unreliable after 21 July 2013; the dashed blue line in Figure 2b indicates the assumed snowmelt progression from then to 23 July, when we estimate that the snowmelt was complete, based on albedo data (see text).

3. Results

3.1. Air Temperature and Surface Conditions

At the SRB/IMB sites, air temperatures were in the −30 to −15°C range in April and then increased to 0°C in late May both in 2012 and 2013 (Figure 2a). Temperatures above 0°C were first reached on 27 May in 2012 and on 3 June in 2013. From late May to 20 June, the air temperature was generally somewhat higher in 2012 than in 2013. Afterward, until 10 August, there was no significant difference between the two years. From 10 August onward, the air temperature dropped below 0°C, followed by intermittent warmer events with temperature rising to nearly 0°C between 18 and 29 August in the two years, even above 0°C in 2013. The summer (June, July, and August—JJA) mean air temperature at the SRB/IMB sites was higher in 2012 (−0.9°C) than 2013 (−1.7°C).

The snow cover evolution was substantially different in 2012 and 2013 at the SRB/IMB sites (Figure 2b), although the surface was covered by snow of similar depth by mid-June in both years. In mid-April, the snow cover was much thicker in 2012 (0.43 m) than in 2013 (0.05 m). From mid-April to 10 June, the snow depth did not change much in 2012, while it increased to about 0.35 m in 2013. After 10 June, snow started to melt in 2012 and had completely melted by 14 July 2012 [see *Wang et al*., 2014]. In 2013, snowmelt onset was around 20 June and snow completely disappeared around 23 July. The assumption of complete disappearance of snow on 23 July is based on the minimum albedo on that date (see section 3.4) [cf. *Wang et al*., 2014]. Thus, starting from the onset of snowmelt it took about 33–35 days for the snow to completely melt in both years. In 2013, the melting of snow was slow when the snow thickness was higher than 0.3 m and became faster when the snow thickness was less than 0.3 m in July. In 2012 the initial snowmelt was quite rapid but was then interrupted by a significant late June snowfall (Figure 2). For most of the snowmelt period, the melt rate was faster in 2012 than in 2013. Most days in 2012 after 10 June had daily melt rates over 1.0 cm d^{-1}, even up to 4 cm d^{-1} at the end of the melt. In 2013, melt rates in late June were less than 1.0 cm d^{-1}, increasing in July, with maximum rates around 3 cm d^{-1}. During the melt season, there were occasional increases in snow depth due to either new snowfall or wind drift in the two summers. The increase was substantial, e.g., in late June 2012, nearly 0.1 m, or minor, e.g., around 10 July in the two years.

Figure 3 shows the time series of TbD extracted along the SRB/IMB drift in 2012 and 2013. Understandably, there are some differences for the exact melt onset date determined from our in situ measurements (single point) and from the satellite data (on larger scale), further complicated by the fact that the passive microwave

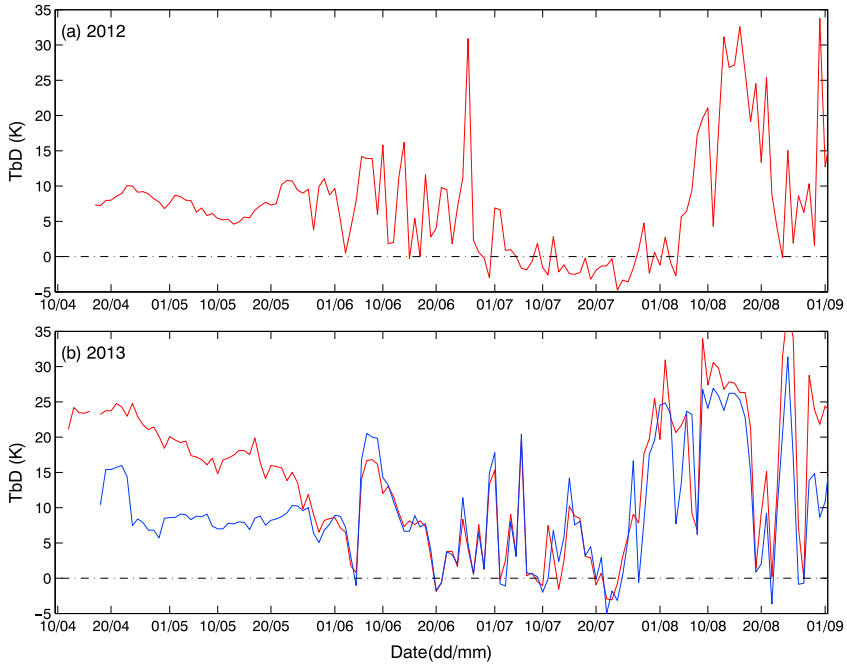

Figure 3. Brightness temperature difference (TbD, as defined in section 2) from SSMIS satellite data in (a) 2012 and (b) 2013, calculated from the pixel nearest the SRB. Prior to 10 June 2012 and 13 June 2013, the SRBs were north of the instrument's field of view (limited to 86.8°N), and the TbD is calculated from the northernmost pixel with SSMIS data at the longitude of the SRB. In Figure 3b the blue line is calculated with 2013 SSMIS data and the 2012 SRB position.

signal is sensitive to melt within the snow pack which can occur before surface melt begins. Nevertheless, the satellite data are useful for getting an idea of the overall length of the melt and how often it was interrupted by surface refreezing events. There was a relatively long period with more or less continuous melt in July 2012 (28 days with TbD less than zero), but a less continuous period of melt in 2013 (12 days with TbD less than zero). In addition, the TbD values frequently showed large positive excursions throughout July 2013, indicating frequent occurrence of surface refreezing. Therefore, there was a longer and more continuous melt period in 2012 than in 2013. To check if the differences in geographical latitude of the buoys positions in the two years had a significant influence on the melt conditions in July, we extracted the TbD in 2013 along the SRB drift locations in 2012 (which were farther south later in the season). This is shown in Figure 3b and indicates that the latitude difference only had a negligible influence on the melt conditions in July. The longer melt season in 2012 was also apparent in the melt pond evolution captured by NPEO webcams (Figure 4). Melt ponds appeared earlier in 2012 (2 July) than in 2013 (8 July), and they refroze later (19 August) in 2012 than in 2013 (3 August). The maximum extent of melt ponds was reached by 14 July 2012 and by 23 July 2013. The fraction of melt ponds seems larger in 2012 than in 2013 in the view of NPEO webcams, although this is difficult to quantify.

3.2. Cloud Cover

From the NPEO webcam images, sky conditions were visually categorized as no clouds (clear sky), partial cloud cover (separately for cloud fractions greater or less than 0.5), or fully overcast. When the webcams were covered by snow or ice, which mostly happened in May, June, and August, the sky condition was categorized as no view. The results are summarized in Figure 5. Between April and August, there were more clear skies in 2012 than in 2013. Clear-sky conditions prevailed more than 60% of the time in April in both years, while nearly 50% of the time in May 2012. In June, the fraction of clear-sky and overcast sky conditions did not differ significantly between the two years. In July, the frequency of clear-sky conditions was similar in 2012 and in 2013, but overcast conditions were more prevalent in 2013. In August, the fraction of overcast conditions was similar between the two years.

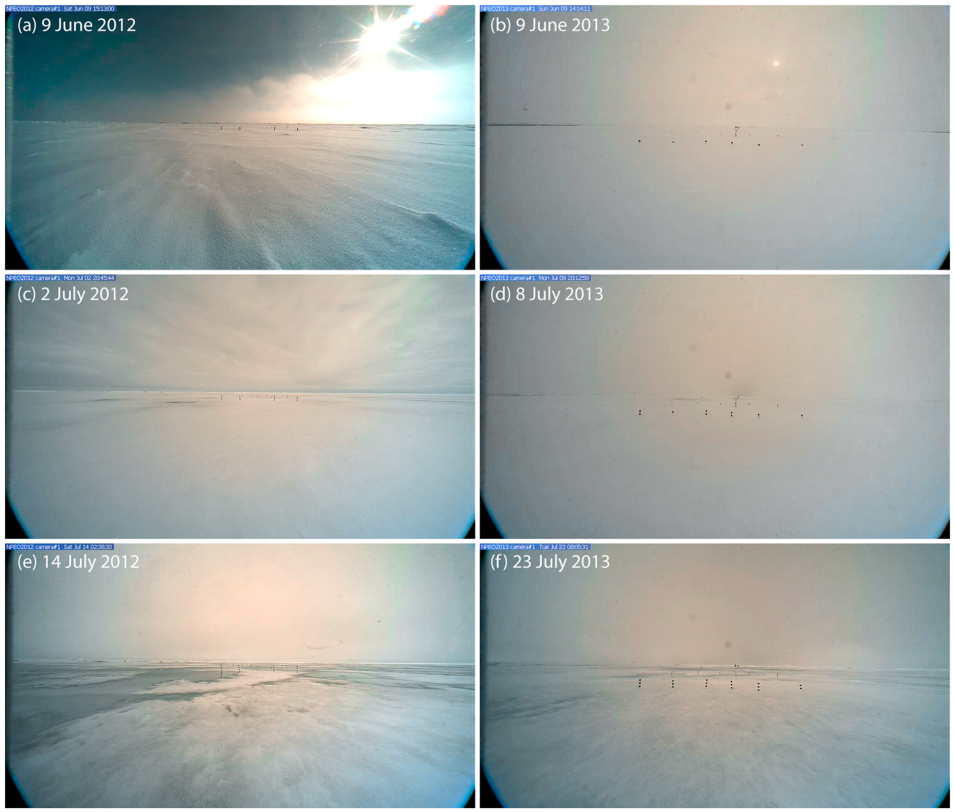

Figure 4. Surface conditions recorded on the days indicated in the photographs by NPEO webcams in 2012 (source: http://psc.apl.washington.edu/northpole/NPEO2012/ARCHIVE/) and 2013 (source: http://psc.apl.washington.edu/northpole/NPEO2013/WEBCAM1/ARCHIVE/).

3.3. In-Band Incident and Reflected Irradiance

There was a general increase in the in-band (350–800 nm) incident light levels from April to June and a decrease thereafter in both 2012 and 2013 (Figure 6a). The reflected irradiance largely demonstrates similar seasonality as the incident in both years (Figure 6c). The incident and reflected light levels in

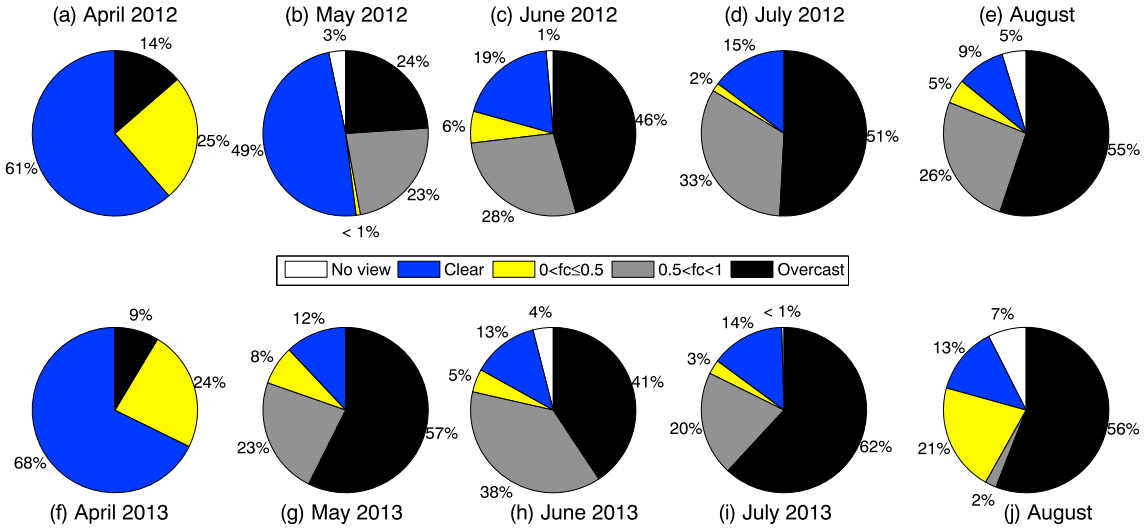

Figure 5. Frequency of different cloud fractions (f_c) (a–e) in 2012 and (f–j) in 2013 estimated from daily NPEO webcam images.

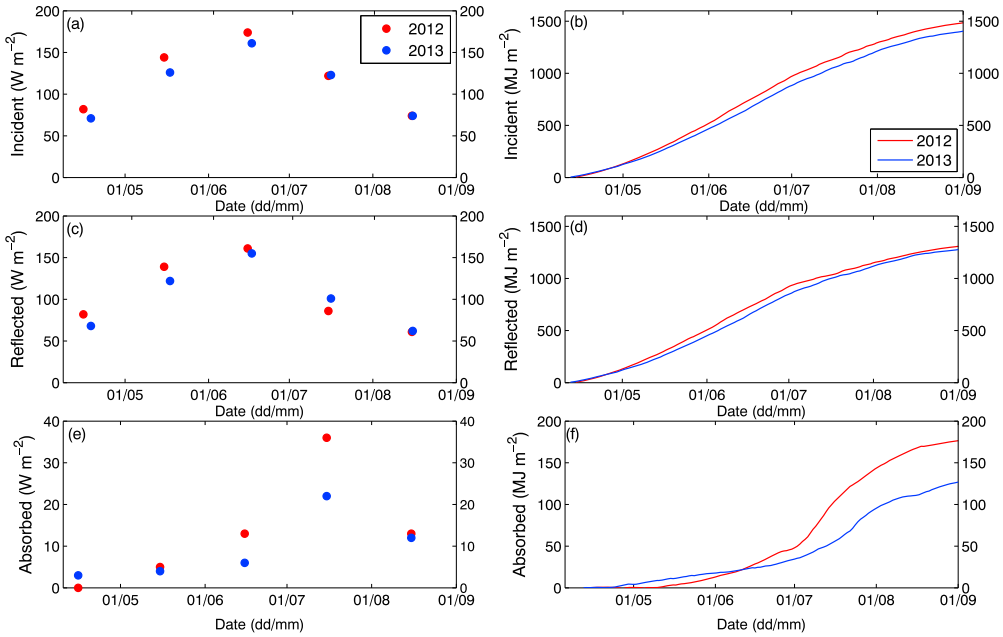

Figure 6. (a, c, and e) Monthly mean and (b, d, and f) cumulative shortwave solar radiation (350–800 nm) incident (Figures 6a and 6b), reflected (Figures 6c and 6d) and absorbed by the ice-ocean system (Figures 6e and 6f) in 2012 (red lines) and in 2013 (blue lines).

April, May, and June were greater in 2012 than in 2013 (Figures 6a and 6c), which resulted in a larger cumulative incident and reflected levels in 2012 than in 2013 (Figures 6b and 6d). There was not a big difference in the incident and reflected light levels in July between the two years. The larger incident levels in April–June 2012 are due to more solar radiation reaching the surface under the more prevalent clear skies in 2012 (Figures 5a–5c). The reflected light levels in July were slightly lower in 2012 than 2013 (Figure 6c). Incident solar radiation not reflected back to the atmosphere accumulates in the ice-ocean system. The solar radiation absorbed by the ice-ocean system is small in April and May and becomes larger between June and August in both years, with a maximum in July (Figure 6e). The accumulated solar energy in the ice-ocean system was slightly lower in May 2012 than in 2013, and after May it was higher in 2012 than in 2013 (Figure 6f).

3.4. In-Band Albedo

The in-band albedo evolution from April to the end of August for both years is shown in Figure 7. In section 4.1, we discuss sources of uncertainty in the data and explain observations of albedos greater than one. In 2012, the surface in-band albedo was above 0.85 until the end of June (see *Wang et al*. [2014] for detailed discussion of the 2012 data). Albedo decreased rapidly in the first half of July, coincident with the loss of snow, and reached the lowest value (0.46) on 14 July, when we assume the last snow disappeared. Afterward, it increased and reached levels above 0.6 by 17 July and returned to nearly premelt values by 20 August. When the albedo was at minimum in 2012, there was likely a mixture of melt pond and bare ice below the SRB sensors [*Wang et al*., 2014]. The albedo in 2013 shows similar seasonality as in 2012 (Figure 7). It is high during the premelt period and begins to decrease in June, coincident with snowmelt onset, first slowly but more quickly when the snow becomes thinner. The albedo reaches a minimum in July, and thereafter, there was a rapid increase in albedo due to changes in the surface state, as described by *Wang et al*. [2014] [cf. *Perovich and Polashenski*, 2012]. After a rapid increase, the albedos gradually return to premelt values. Episodic summer snowfall can lead to substantial increase in albedo, for example, around 10 July in both 2012 and 2013, a few centimeters of new snow resulted in albedo increases of about 0.2, indicating the importance of episodic summer snowfall for albedo.

There were, however, significant differences of the albedo in the two years: (1) in 2012, the fastest decrease of albedo was in the first half of July, while in 2013 it was in the second half of July; (2) the period with low albedo was longer and more pronounced in 2012 than in 2013; (3) the lowest values of surface albedo were

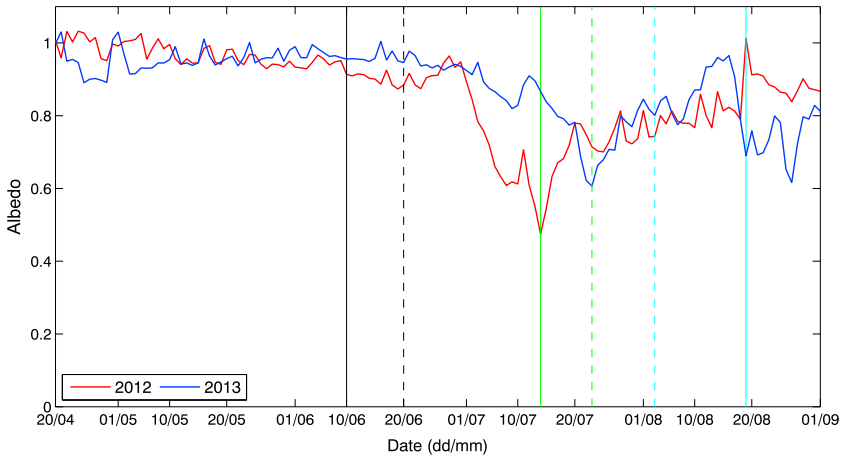

Figure 7. Time series of daily in-band albedo in 2012 (red) and 2013 (blue) between 20 April and 31 August. Spectra with albedos greater than one can occur due to small errors in observations with very high albedo conditions combined with low Sun angles [*Nicolaus et al*., 2010a; *Wang et al*., 2014]. Vertical lines are the dates of snowmelt onset (black), snow complete disappearance (green), and refreeze-up (cyan) in 2012 (solid lines) and 2013 (dashed lines).

observed on 14 July 2012, but not until 23 July 2013, which is likely the time when all snow had melted. During the melt season, the albedo was lower in 2012 than in 2013, although a direct comparison of the absolute albedo values is hampered by the fact that the surface conditions directly under the SRB sensors were likely different in 2012 and 2013. This difference shows how the location of the buoy relative to small-scale melt features on the surface can be a challenge.

4. Discussion

4.1. Uncertainties in Radiation Measurements

Small errors in observations with very high albedo conditions, especially when combined with low Sun angles, can cause albedos to appear to exceed one. One way this could happen is through the accumulation of snow, frost, or water on the above-ice sensors, most often on the incident sensor [*Nicolaus et al*., 2010a; *Wang et al*., 2014]. This results in artificial temporary decreases in incident irradiance and increases in albedo. As long as this accumulation is naturally removed through melt, sublimation, or evaporation, the seasonal evolution of the albedo can still be estimated by ignoring the temporary positive albedo deviations. Observations made with similar flat cosine sensors to those used here, but at manned locations [e.g., *Nicolaus et al*., 2010b], show that even when unheated and unventilated, these sensors are much more resistant to accumulation or deposition than traditional glass-dome sensors and that they have a self-cleaning capacity through absorption of sunlight by the black case.

Another source of uncertainty in unmanned radiation measurements results from the possibility that the sensors or surface below them become tilted or sloped. This changes the effective solar zenith angle, introducing an artificial diurnal cycle in the measured incident irradiance (for sensor tilt) or reflected irradiance (for surface slope). Frequent cloud cover over the Arctic Ocean helps alleviate tilt errors by diffusing the incident radiation. Surface slopes on level sea ice are generally small compared to the sastrugi that form on ice sheets, and the sensors recorded their tilt, reporting less than 2°. At large solar zenith angles, such small tilts or slopes can cause significant relative errors in the observations under direct sunlight; however, an examination of the diurnal cycle in the data does not show any obvious problems. We have also chosen to work with albedo data observed at solar noon to minimize the solar zenith angle, especially later in the melt season, when the most interesting changes happen. Replotting Figure 7 with daily mean data (not shown) does not change the interpretation of the seasonal cycle, which is encouraging since tilt effects will be averaged out to a large degree in the daily mean since the cosine function is nearly linear over our range of solar zenith angles. In the end, we have chosen to use the solar noon data because they are least affected by shadowing (the sensors extended south of the support structure, and rotation appears to have been minimal), and the increased incident irradiance at that time may reduce the likelihood of ice accumulation on the sensors, as discussed above.

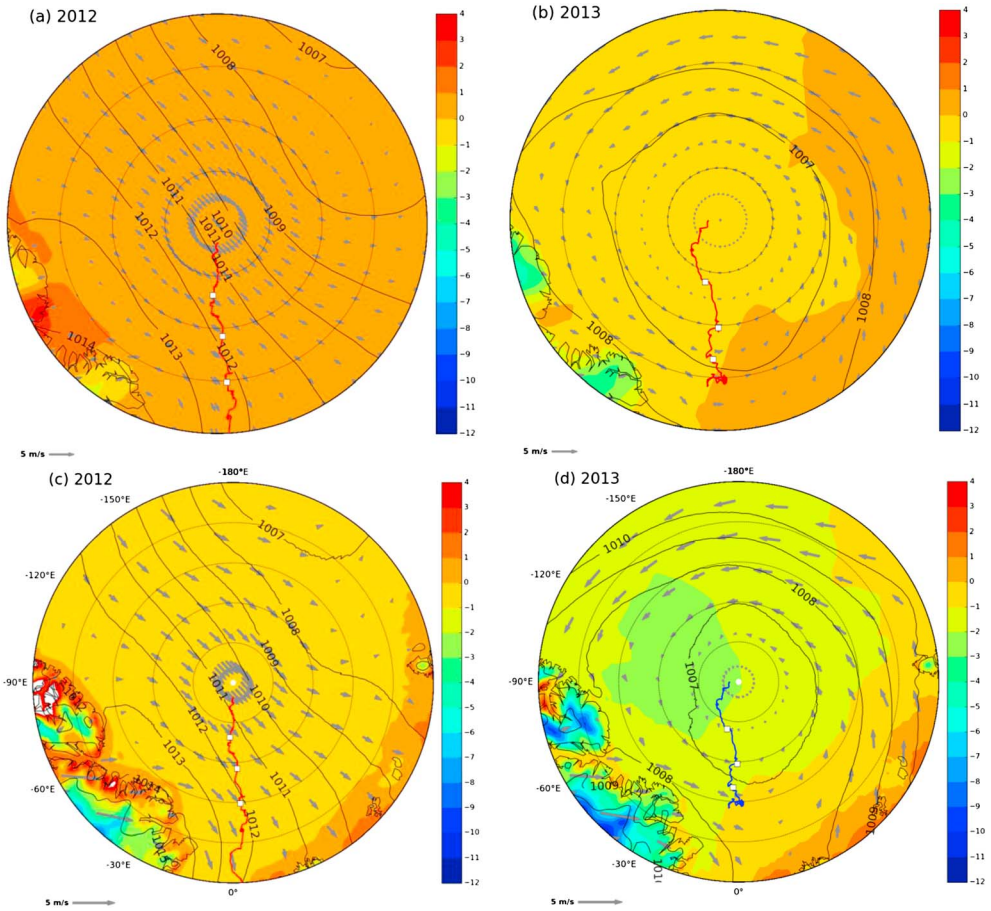

Figure 8. Summer (JJA) mean 2 m air temperature (°C, color shading), 10 m wind (vectors, scale shown at the bottom left corner of the graphs), and SLP (hPa, black contours) in 2012 and 2013 (a and b) from ERA-Interim reanalysis data and (c and d) from CFSv2 analysis data. The red lines are the trajectories of our buoys, with white markers for 1 June, 1 July, and 1 August from north to south.

4.2. Atmospheric Conditions in Summer 2012 and 2013 From ERA-Interim and CFSv2

Atmospheric conditions over the central Arctic were different in summers 2012 and 2013 (Figure 8). The mean SLP over the region in summer 2012 was characterized by a dipole pattern, with high SLP over the western Arctic and low SLP over the eastern Arctic [see also *Overland et al*., 2012], while in summer 2013 it was characterized by a low-pressure area centered over the Arctic [see also *Overland et al*., 2013]. These SLP patterns facilitated more warm air advection from lower latitudes into the Arctic in 2012 than in 2013. The ERA-Interim reanalysis data show a slightly higher air temperature than the CFSv2 analysis data [*Jakobson et al*., 2012]. However, both data sets show that the mean air temperature in the summer (JJA) was higher in 2012 than in 2013 over most of the central Arctic Basin (Figure 8), including the SRB/IMB region (see section 3.2). This difference is in line with in situ data from the IMB buoy and the TbD analysis from satellite observations, which indicated a shorter melt period in 2013, frequently interrupted by refreezing. On average, winds in summer were from the north in 2012 but from the west and weaker in 2013 in the SRB/IMB region, supporting the enhanced ice drift speed in 2012 (Figure 1). An unprecedented strong storm entered the central Arctic in early August 2012 [*Simmonds and Rudeva*, 2012]. Although this storm did not directly affect the SRB/IMB region, it accelerated the Arctic-wide ice loss in summer 2012. Under the effect of the strong storm, the already relatively thin Arctic ice pack was made more vulnerable to melt due to stronger upward ocean heat transport, more ice motion and hence deformation due to strong wind, and more exposure to wind and waves, facilitating the main ice pack's further decay [*Parkinson and Comiso*, 2013; *Zhang et al*., 2013].

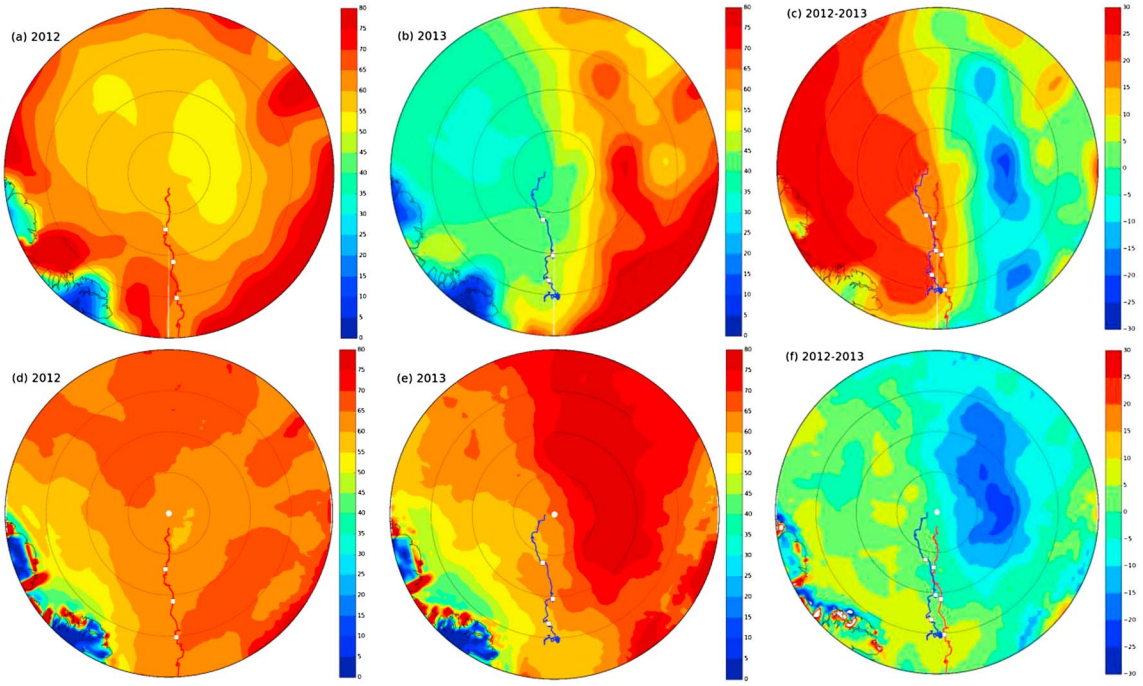

Figure 9. Summer mean (JJA) of netF (a and d) in 2012, (b and e) in 2013 and (c and f) their difference between 2012 and 2013, based on ERA-Interim reanalysis data (Figures 9a–9c) and CFSv2 analysis data (Figures 9d–9f); all units are W m^{-2}. The red/blue lines are SRB/IMB tracks in 2012/2013.

4.3. Surface Energy Budget From ERA-Interim and CFSv2

Figure 9 shows the mean summer (JJA) netF (net heat flux to the surface) over the Arctic Ocean in 2012 and 2013, and the difference between 2012 and 2013, based on ERA-Interim reanalysis and CFSv2 analysis data. In the Arctic, netF is typically negative from August to May and positive from May to August [*Maksimovich and Vihma*, 2012] (also see Figure 10). A detailed comparison of ERA-

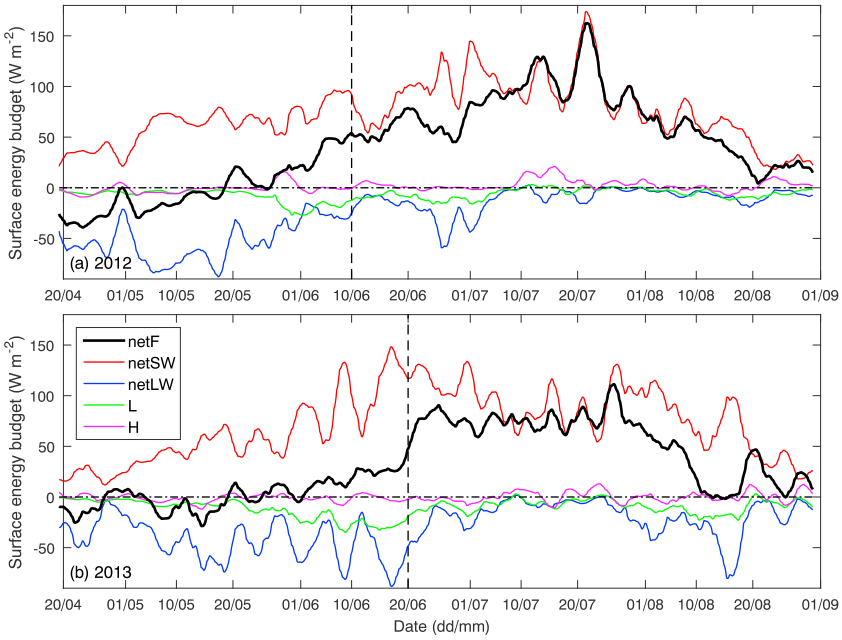

Figure 10. Surface energy budget terms in (a) 2012 and (b) 2013 at the SRB/IMB sites based on ERA-Interim reanalysis data. The vertical black dashed lines indicate the dates of the snowmelt onset, and horizontal dash-dotted black lines denote zero surface energy budget.

Interim and CFSv2 is not in the scope of this study. However, we do see that the summer mean netF has a similar pattern in both data sets, although the summer mean netF was slightly larger in the CFSv2 than in the ERA-Interim. The summer mean netF was positive over all of the Arctic Ocean in the summers of 2012 and 2013 (Figures 9a, 9b, 9d, and 9e) in both ERA-Interim and CFSv2, indicating heating or melting at the surface of the Arctic Ocean. The difference between netF in the two summers (2012 minus 2013) is about 10–20 W m^{-2} in the ERA-Interim and 0–10 W m^{-2} in the CFSv2 in our SRB/IMB region (Figure 9c), consistent with our observations that there was more melting in 2012 than in 2013.

In the Arctic, the turbulent heat fluxes (L + H), in particular H, are small as shown by ERA-Interim (Figure 10), playing a minor role in the surface energy budget [*Persson et al*., 2002; *Hudson et al*., 2013], while the netSW and netLW are the two main terms of netF, being tens of W m^{-2} (Figure 10). In both years, netSW was low in April and increased into June and July, as incoming solar radiation increased and surface albedo decreased. However, in 2012, there was a strong longwave cooling in April and May, but weak cooling in June, July, and August, driven by the clear-sky conditions in April and May and cloudier conditions in June, July, and August (Figure 5). In 2013, there was significant intermittent longwave cooling between mid-May and mid-June, and weak longwave cooling between late April and early May and between late June and July driven by sky conditions. While the clear skies that promote enhanced longwave cooling also lead to increased incident solar radiation, the high premelt albedo reduces the effect on net shortwave heating to some extent; furthermore, longwave radiation is absorbed and emitted at the snow surface, while shortwave radiation is absorbed through the depth of snow and ice, making the longwave cooling efficient at keeping the surface from melting. The timing of snowmelt onset observed at the SRB/IMB sites corresponds quite well with the transition from strong to weak longwave loss, indicating the key role of longwave radiation in initiating snowmelt [*Maksimovich and Vihma*, 2012; *Else et al*., 2014]. This suggests that the clear periods in early and mid-June 2013 may have helped delay the melt onset and the associated albedo reduction and warming feedback. In the next sections, we will examine the importance of this delay.

4.4. Observed Shortwave Albedo Evolution in Summer 2012 and 2013

The observed in-band albedo was somewhat higher in 2013 than in 2012. The spectral albedo (not shown) at longer wavelengths (700–800 nm) never dropped below 0.4 after the snow completely disappeared in 2013, as it did in 2012. This suggests that there were likely no melt ponds [*Hanesiak et al*., 2001], but only bare ice immediately around the 2013 SRB site. The lower albedo values for a longer period in July 2012 than in 2013 are also indicative of generally more pronounced and continuous surface melting in 2012, as indicated by higher TbD values and higher air temperatures in 2012. Thus, the evolution of surface albedo in 2012 and 2013 represents two different cases, one with a mixed surface of melt pond and bare ice and a longer melt season, the other with predominantly bare ice and a shorter period of low albedo.

The albedo evolution observed in this study is an intermediate case between the seasonal ice and MYI (at lower latitudes) described by *Perovich and Polashenski* [2012]. FYI drifting over the North Pole survives the melt season while drifting to the south, then becoming second-year ice [*Perovich et al*., 2014a; *Wang et al*., 2014]. Since refreezing begins before the ice completely melts, the albedo never approaches that of open water, as it does in *Perovich and Polashenski's* [2012] truly seasonal case. Thus, the seasonality and evolution of albedo on FYI in the central Arctic today more closely resembles their case for MYI, but with shifts toward lower albedo and higher transmission. Cases A and B in Figure 11a are idealizations of the observed albedo evolution in 2012 and 2013, respectively.

4.5. Effect of Albedo Seasonality

The seasonal evolution of albedo greatly influences the solar heat input to the ice-ocean system [cf. *Perovich et al*., 2007, 2011a; *Wang et al*., 2014]. We illustrate this by considering the two idealized cases A and B, which were largely controlled by the prevailing atmospheric and surface conditions. The observed in-band incident solar radiation in 2012 from 20 April to the end of August (Figure 11b) is used to calculate the in-band solar heat input to the ice-ocean system, $Q_s = (1 - \alpha)F_r$, where F_r is the daily incident in-band solar radiation and α is the albedo from cases A and B.

Prior to snowmelt onset, the majority (over 90%) of the incident in-band solar radiation is reflected back to the atmosphere. Most of the energy input to the ice-ocean system is between June and July (Figure 11c),

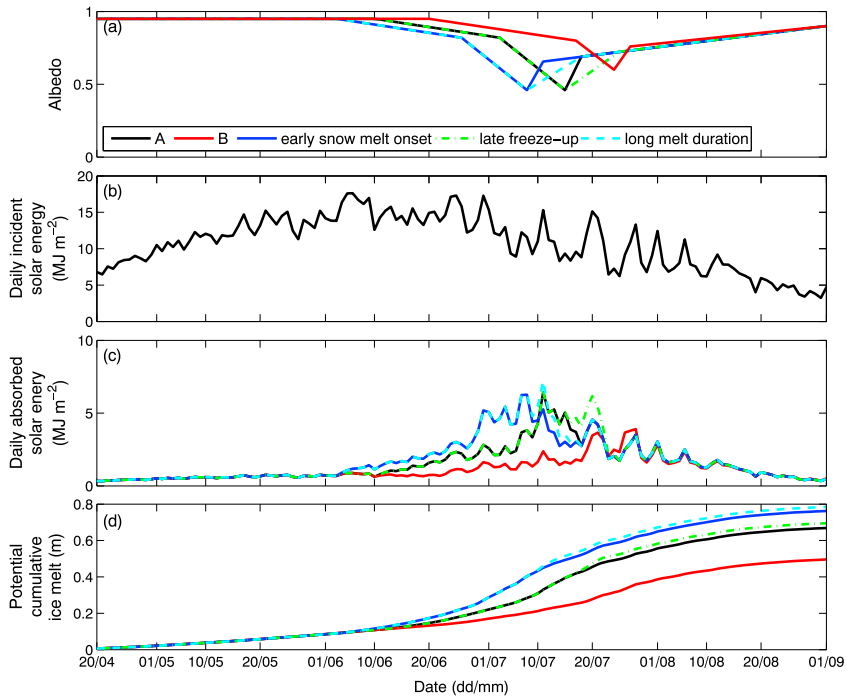

Figure 11. Time series of (a) the idealized evolution of albedo, (b) observed daily incident in-band solar radiation in 2012, (c) daily solar in-band energy input, and (d) potential ice melt for five idealized cases. Case A is based on 2012 observations; case B is based on 2013 observations; the other three cases: early melt onset represents snowmelt onset 1 week earlier than case A, late freeze-up is freeze-up 1 week later than case A, and long melt duration describes snowmelt onset 1 week earlier and freeze-up 1 week later than case A; thus, melt duration is 2 weeks longer than in case A.

once snow and ice albedo has decreased and the incident solar radiation is large. The solar in-band energy input decreases in August when the incident solar radiation decreases and the albedo increases. The solar energy input to the ice-ocean system in the two cases starts to diverge from 10 June onward, once snowmelt begins in case A. The integrated in-band solar heat input to the ice-ocean system increases slowly from April to early June, then more rapidly in late June and July in both cases.

The absorbed in-band solar energy in June, July, and August is 87% (case A) and 83% (case B) of the total accumulated energy between April and August. Thus, solar energy deposition mainly takes place between June and August. By 31 August, the integrated in-band solar energy in the ice-ocean system is 205 MJ m^{-2} in case A and 152 MJ m^{-2} in case B. About 3 MJ m^{-2} is required to melt 1 cm of pure ice (assuming a latent heat of fusion of 334,000 J kg^{-1} and a density of 917 kg m^{-3}). Thus, the amount of potential ice melt in cases A and B, if all of the solar energy absorbed in the ocean is used for melt, corresponds to 0.68 m and 0.51 m, respectively (Figure 11d). This difference is due entirely to the albedo differences caused by the shorter and less pronounced melt season of case B, showing that any factors that act to shorten or lessen the severity of the surface melt will be significantly amplified through the resulting effect on albedo.

4.6. Importance of the Timing of Snowmelt to the Solar Energy Input in the Ice-Ocean System

The timing of snowmelt onset is important for the total solar energy accumulation in the ice-ocean system since it triggers the initial albedo decrease [*Perovich et al.*, 2007; *Arndt and Nicolaus*, 2014]. To investigate how the timing of snowmelt influences the solar energy input to the ice-ocean system, separately from other differences in the melt season, we consider three additional cases: snowmelt onset 1 week earlier than in case A ("early snowmelt onset" case), freeze-up 1 week later than in case A ("late freeze-up" case), and snowmelt onset 1 week earlier and freeze-up 1 week later than in case A ("longer melt duration" case). In the early snowmelt onset case, an additional 14% (or 29 MJ m^{-2}) of in-band solar heat is deposited in the ice-ocean system, equivalent to 0.10 m of potential ice melt (Figure 11d). In the late freeze-up case, the accumulated solar heat input to the ice-ocean system is 8 MJ m^{-2} or 4% higher than in case A. In the longer melt duration case, the

melt season is 2 weeks longer than in case A, and the accumulated solar energy in the ice-ocean system is 17% or 35 MJ m^{-2} more than in case A.

These results, which neglect the additional effect that the minimum albedo would likely be lower as a result of the additional melt in the early onset case, show that the timing of melt onset is far more important to the total amount of solar in-band energy input during the melt season than the timing of freeze-up. This is because incident solar radiation is much larger in May and June than in August (Figure 6a) [*Ebert and Curry*, 1993; *Perovich et al*., 2007; *Maksimovich and Vihma*, 2012], and a change of the timing of melt onset propagates through the entire melt season [*Perovich et al*., 2007]. Therefore, the fact that snowmelt onset was about 10 days earlier in 2012 than in 2013 greatly increased the likelihood that 2012 would have a more pronounced melt season overall than 2013.

4.7. Out-of-Band Radiation, Open Water, and Leads

The calculations in sections 4.4 and 4.5 show the importance of the melt onset date in a relatively simple manner using idealized scenarios based on modifications to the observed albedo seasonality in 2012. The goal was not to quantify the exact impact of the changes to the melt season but to see their relative importance. These simple calculations show the importance of the melt onset date for the overall melt season, but they do leave out some important factors, which we briefly consider here.

In sections 4.4 and 4.5, leads and other areas of open water were neglected. In the central Arctic, the open water fraction is typically small (often less than 10%), but the fact that open water absorbs 2 to 3 times as much broadband solar radiation as bare ice means that these small areas can contribute significantly to the overall uptake of solar radiation in the region. Changes that increase the amount of melt, such as an earlier melt onset, will lead to thinner ice that can more easily allow the dynamic formation of leads or be completely melted through. More FYI could also result in more expansive melt ponds [*Polashenski et al*., 2012], which in turn are important for the evolution of ice extent [*Schröder et al*., 2014; *Liu et al*., 2015]. These effects will further enhance the importance of an earlier melt onset, beyond what is discussed above.

Sections 4.4 and 4.5 only consider in-band (350–800 nm) solar radiation. While this wavelength range includes the majority of incident solar radiation [e.g., *Grenfell and Perovich*, 1984, 2008], the much lower albedo of ice and snow at longer wavelengths means that a large portion of the absorbed solar radiation is often at longer wavelengths. For example, for the average spectral albedo and incident irradiance observed by *Hudson et al*. [2012, their Figure 7] on a partly cloudy day in June on sea ice near Barrow, Alaska, about 65% of incident solar radiation was between 350 and 800 nm, but only about half of the absorbed radiation was in this wavelength range (averaged over a mix of bare ice and melt ponds). The higher the visible albedo, the greater the fraction of out-of-band absorbed radiation. Thus, for bare unponded ice, somewhat more than half of the absorbed radiation is at wavelengths longer than 800 nm, and for snow-covered ice (with high visible albedo), nearly all of the absorbed radiation can be at longer wavelengths, even for melting snow [*Grenfell and Maykut*, 1977; *Wiscome and Warren*, 1980; *Aoki et al*., 2003; *Grenfell and Perovich*, 2004].

Neglecting the out-of-band radiation in the sections above clearly limits the quantitative interpretation of the results there, but the qualitative conclusions remain. To investigate the out-of-band effects, we looked at the amount of light absorbed by dry snow, bare melting ice, and melt ponds under the clear-sky incident spectrum used by *Hudson et al*. [2012] (Figure S1 in the supporting information, albedo spectra for bare ice and ponds were also taken from *Hudson et al*. [2012]; the spectral albedo of snow was modeled). At wavelengths longer than 1400 nm, there is essentially no change in absorbed radiation as the surface changes from snow to pond. When shifting from snow to bare ice, roughly one third of the additional absorption occurs between 800 and 1400 nm; going from bare ice to pond, roughly one quarter of the additional absorption is in that region. Therefore, while the calculations above ignore the melting caused by longer wavelength solar radiation, they capture the largest part of the feedback caused by an earlier melt onset or longer melt season, but they do underestimate the overall effect.

5. Conclusions

The Arctic sea ice extent was lower in summer 2012 (so far the lowest recorded in the Arctic since satellite observations started 1979) than in summer 2013. Autonomous systems of SRBs and IMBs were deployed in the central Arctic in the two years from spring to fall to observe the seasonal evolution of solar radiation, and snow and

sea ice mass balance. Complemented with ERA-Interim reanalysis, CFSv2 analysis, and satellite passive microwave data, we presented the surface and atmospheric conditions, as well as their influence on the ice-ocean system in the high Arctic in the two summers. Although our solar radiation observation was limited to wavelengths 350–800 nm, neglecting radiation at longer wavelengths did not change our qualitative results, since solar radiation at shorter wavelengths causes large absolute and relative changes in the amount of energy absorbed. We found that the surface conditions, the atmospheric circulation patterns, and the net surface energy balance were quite different between the years, at least, in the region covered by our autonomous observations. This is also reflected in the observations of surface albedo and ice melt. The conditions in 2012 exhibited a longer and more continuous period of ice and snowmelt, with earlier melt onset and later freeze-up than in 2013, resulting in more ice melt in 2012 than in 2013 [see *Perovich et al*., 2014a].

Snow plays an important role in reducing the solar heat accumulation in the ice-ocean system. Snowmelt onset is strongly influenced by longwave radiative cooling of the surface, one of the two main terms of the surface heat budget in the Arctic summer. The timing of this melt onset is more important to the solar heat input to the ice-ocean system than the timing of freeze-up [cf. *Perovich et al*., 2007]. A 1 week earlier snowmelt onset results in about 14% more in-band solar energy accumulation in the ice-ocean system, roughly 0.10 m of ice melt. Episodic summer snowfall can substantially increase the albedo, decreasing the solar heat input to the ice-ocean system (at least transiently but at time when incident shortwave radiation is high). Thus, it is important to accurately represent summer snowfall events in climate system models [*Light et al*., 2015b].

The earlier melt onset in 2012 likely preconditioned the system to allow a longer melt season with lower albedo, resulting in much more solar heat input to the ice-ocean system in 2012 than in 2013. This additional deposited solar energy would melt the surface, thin the ice, and warm the upper ocean, resulting in more melting and longer melt period. This enhances the positive ice-albedo feedback. This also helps explain the increased melting in 2012 versus 2013 as shown in this study, and more substantial surface and bottom ice melting in 2012 than 2013 as indicated by *Perovich et al*. [2014a].

Acknowledgments

The authors are grateful to Marius Bratrein, Jago Wallenschus, Tor Ivan Karlsen, and Kristen Fossan at Norwegian Polar Institute (NPI) for their work with SRB design, construction, and deployments. We also wish to acknowledge National Snow and Ice Data Center for providing SSMIS data, ECWMF for ERA-Interim data, NCEP for CFSv2 data, and North Pole Environmental Observatory (NPEO), University of Washington, USA, for webcam photos. This study was supported by the Research Council of Norway through projects AMORA (project 193592) and STASIS (project 221961/F20), by the Fram Centre "Arctic Ocean" flagship program through the SOLICE project, by Centre for Ice, Climate and Ecosystems (ICE) at NPI, and by ACCESS, a European project within the Ocean of Tomorrow call of the European Commission Seventh Framework Programme (grant 265863). Solar radiation data are available on request to data@npolar.no, and snow and ice mass balance data can be found at http://imb.erdc.dren.mil/buoysum.htm. Constructive comments from two anonymous reviewers aided to improve the paper.

References

Anderson, M., A. C. Bliss, and S. Drobot (2014), *Snow Melt Onset Over Arctic Sea Ice From SMMR and SSM/I-SSMIS Brightness Temperature*, version 3, NASA National Snow and Ice Data Center Distributed Active Archive Center, Boulder, Colo. [Available at 10.5067/22NFZL42RMUO.]

Aoki, T., A. Hachikubo, and M. Hori (2003), Effects of snow physical parameters on shortwave broadband albedos, *J. Geophys. Res.*, *108*(D19), 4616, doi:10.1029/2003JD003506.

Arndt, S., and M. Nicolaus (2014), Seasonal cycle and long-term trend of solar energy fluxes through Arctic sea ice, *Cryosphere*, *8*, 2219–2233. [Available at www.the-cryosphere.net/2219/2014/doi:10.5194/tc-8-2219-2014.]

Arrigo, K. R., et al. (2012), Massive phytoplankton blooms under Arctic sea ice, *Science*, *336*(6087), 1408, doi:10.1126/science.1215065.

Bliss, A. C., and M. R. Anderson (2014), Snowmelt onset over Arctic sea ice from passive microwave satellite data: 1979–2012, *Cryosphere*, *8*, 2089–2100, doi:10.5194/tc-8-2089-2014.

Brown, Z. W., and K. R. Arrigo (2013), Sea ice impacts on spring bloom dynamics and net primary production in the Eastern Bering Sea, *J. Geophys. Res. Oceans*, *118*, 43–62, doi:10.1029/2012JC008034.

Cavalieri, D., P. Gloerson, and J. Zwally (1990, 2014), *DMSP SSM/I-SSMIS Daily Polar Gridded Sea Ice Concentrations, [2012–2013]*, edited by J. Maslanik and J. Stroeve, National Snow and Ice Data Center. Digital media, Boulder, Colo.

Comiso, J. C., C. L. Parkinson, R. Gersten, and L. Stock (2008), Accelerated decline in the Arctic sea ice cover, *Geophys. Res. Lett.*, *35*, L01703, doi:10.1029/2007GL031972.

Dee, D. P., and S. Uppala (2009), Variational bias correction of satellite radiance data in the ERA-Interim reanalysis, *Q. J. R. Meteorol. Soc.*, *135*(644), 1830–1841, doi:10.1002/qj.493.

Dee, D. P., et al. (2011), The ERA-Interim reanalysis: Configuration and performance of the data assimilation system, *Q. J. R. Meteorol. Soc.*, *137*, 553–597, doi:10.1002/qj.828.

Ebert, E. E., and J. A. Curry (1993), An intermediate one-dimensional thermodynamic sea-ice model for investigating ice-atmosphere interactions, *J. Geophys. Res.*, *98*(C6), 10,085–10,109, doi:10.1029/93JC00656.

Else, B. G. T., T. N. Papakyriakou, R. Raddatz, R. J. Galley, C. J. Mundy, D. G. Barber, K. Swystun, and S. Rysgaard (2014), Surface energy budget of landfast sea ice during the transitions from winter to snowmelt and melt pond onset: The importance of net longwave radiation and cyclone forcings, *J. Geophys. Res. Oceans*, *119*, 3679–3693, doi:10.1002/2013JC009672.

Grenfell, T. C., and G. A. Maykut (1977), The optical properties of ice and snow in the Arctic basin, *J. Glaciol.*, *18*(80), 445–463.

Grenfell, T. C., and D. K. Perovich (1984), Spectral albedos of sea ice and incident solar irradiance in the Southern Beaufort Sea, *J. Geophys. Res.*, *89*(C3), 3573–3580, doi:10.1029/JC089iC03p03573.

Grenfell, T. C., and D. K. Perovich (2004), Seasonal and spatial evolution of albedo in a snow-ice-land-ocean environment, *J. Geophys. Res.*, *109*, C01001, doi:10.1029/2003JC001866.

Grenfell, T. C., and D. K. Perovich (2008), Incident spectral irradiance in the Arctic Basin during the summer and fall, *J. Geophys. Res.*, *113*, D12117, doi:10.1029/2007JD009418.

Haas, C., A. Pfaffling, S. Hendricks, L. Rabenstein, J.-L. Etienne, and I. Rigor (2008), Reduced ice thickness in Arctic Transpolar Drift favors rapid ice retreat, *Geophys. Res. Lett.*, *35*, L17501, doi:10.1029/2008GL034457.

Hanesiak, J. M., D. G. Barber, R. A. De Abreu, and J. J. Yackel (2001), Local and regional albedo observations of Arctic first-year sea ice during melt ponding, *J. Geophys. Res.*, *106*(C1), 1005–1016, doi:10.1029/1999JC000068.
Hansen, E., S. Gerland, M. A. Granskog, O. Pavlova, A. H. H. Renner, J. Haapala, T. B. Løyning, and M. Tschudi (2013), Thinning of Arctic sea ice observed in Fram Strait : 1990–2011, *J. Geophys. Res. Oceans*, *118*, 5202–5221, doi:10.1002/jgrc.20393.
Hudson, S. R., M. A. Granskog, T. I. Karlsen, and K. Fossan (2012), An integrated platform for observing the radiation budget of sea ice at different spatial scales, *Cold Reg. Sci. Technol.*, *82*, 14–20.
Hudson, S. R., M. A. Granskog, A. Sundfjord, A. Randelhoff, A. H. H. Renner, and D. V. Divine (2013), Energy budget of first-year Arctic sea ice in advance stages of melt, *Geophys. Res. Lett.*, *40*, 2579–2583, doi:10.1002/grl.50517.
Jakobson, E., T. Vihma, T. Palo, L. Jakobson, H. Keernik, and J. Jaagus (2012), Validation of atmospheric reanalyses over the central Arctic Ocean, *Geophys. Res. Lett.*, *39*, L10802, doi:10.1029/2012GL051591.
Jeffries, M., and J. Richter-Menge (2013), The Arctic (in "State of the Climate in 2012"), *Bull. Am. Meteorol. Soc.*, *94*, S126–S128.
Jeffries, M. O., J. A. Richter-Menge, and J. E. Overland (Eds.) (2013), Arctic Report Card 2013. [Available at http://www.arctic.noaa.gov/reportcard.]
Kwok, R., and D. A. Rothrock (2009), Decline in Arctic sea ice thickness from submarine and ICESat records: 1958–2008, *Geophys. Res. Lett.*, *36*, L15501, doi:10.1029/2009GL039035.
Laxon, S. W., et al. (2013), CryoSat-2 estimates of Arctic sea ice thickness and volume, *Geophys. Res. Lett.*, *40*, 732–737, doi:10.1002/grl.50193.
Light, B., T. C. Grenfell, and D. K. Perovich (2008), Transmission and absorption of solar radiation by Arctic sea ice during the melt season, *J. Geophys. Res.*, *113*, C03023, doi:10.1029/2006JC003977.
Light, B., D. K. Perovich, M. Webster, C. Polashenski, and R. Dadic (2015a), Optical properties of melting first-year Arctic sea ice, *J. Geophys. Res. Oceans*, *120*, 7657–7675, doi:10.1002/2015JC011163.
Light, B., S. Dickinson, D. K. Perovich, and M. M. Holland (2015b), Evolution of summer Arctic sea ice albedo in CCSM4 simulations: Episodic summer snowfall and frozen summers, *J. Geophys. Res. Oceans*, *120*, 284–303, doi:10.1002/2014JC010149.
Liu, J., M. Song, R. M. Horton, and Y. Hu (2015), Revisiting the potential of melt pond fraction as a predictor for the seasonal Arctic sea ice extent minimum, *Environ. Res. Lett.*, *10*, 05407, doi:10.1088/1748-9326/10/5/054017.
Maksimovich, E., and T. Vihma (2012), The effect of surface heat fluxes on interannual variability in the spring onset of snow melt in the central Arctic Ocean, *J. Geophys. Res.*, *117*, C07012, doi:10.1029/2011JC007220.
Markus, T., J. C. Stroeve, and J. Miller (2009), Recent changes in Arctic sea ice melt onset, freezeup, and melt season length, *J. Geophys. Res.*, *114*, C12024, doi:10.1029/2009JC005436.
Maslanik, J., and J. Stroeve (1990, 2014), *DMSP SSM/I-SSMIS Daily Polar Gridded Brightness Temperatures, 2012–2013*, Natl. Snow and Ice Data Center. Digital media, Boulder, Colo.
Maslanik, J., J. Stroeve, C. Fowler, and W. Emery (2011), Distribution and trends in Arctic sea ice age through spring 2011, *Geophys. Res. Lett.*, *38*, L13502, doi:10.1029/2011GL047735.
Maslanik, J. A., C. Fowler, J. Stroeve, S. Drobot, J. Zwally, D. Yi, and W. Emery (2007), A younger, thinner Arctic ice cover: Increased potential for rapid, extensive sea-ice loss, *Geophys. Res. Lett.*, *34*, L24501, doi:10.1029/2007GL032043.
Nghiem, S. V., I. G. Rigor, D. K. Perovich, P. Clemente-Colón, J. W. Weatherly, and G. Neumann (2007), Rapid reduction of Arctic perennial sea ice, *Geophys. Res. Lett.*, *34*, L19504, doi:10.1029/2007GL031138.
Nicolaus, M., S. Gerland, S. R. Hudson, S. Hanson, J. Haapala, and D. K. Perovich (2010a), Seasonality of spectral albedo and transmittance as observed in the Arctic Transpolar Drift in 2007, *J. Geophys. Res.*, *115*, C11011, doi:10.1029/2009JC006074.
Nicolaus, M., S. R. Hudson, S. Gerland, and K. Munderloh (2010b), A modern concept for autonomous and continuous measurements of spectral albedo and transmittance of sea ice, *Cold Reg. Sci. Technol.*, *62*, 14–28, doi:10.1016/j.coldregions.2010.03.001.
Nicolaus, M., C. Katlein, J. Maslanik, and S. Hendricks (2012), Changes in Arctic sea ice in increasing light transmittance and absorption, *Geophys. Res. Lett.*, *29*, L24501, doi:10.1029/2012GL053738.
Overland, J., J. Key, B.-M. Kim, S.-J. Kim, Y. Liu, J. Walsh, M. Wang, and U. Bhatt (2012), Air temperature, atmospheric circulation and clouds [in Arctic Report Card 2012]. [Available at http:www.arctic.noaa.gov/reportcard.]
Overland, J., E. Hanna, I. Hanssen-Bauer, B.-M. Kim, S.-J. Kim, J. Walsh, M. Wang, and U. Bhatt (2013), Air temperature [in Arctic Report Card 2013]. [Available at http:www.arctic.noaa.gov/reportcard.]
Parkinson, C. L., and J. C. Comiso (2013), On the 2012 record low Arctic sea ice cover: Combined impact of preconditioning and an August storm, *Geophys. Res. Lett.*, *40*, 1356–1361, doi:10.1002/grl.50349.
Perovich, D. K., and C. Polashenski (2012), Albedo evolution of seasonal Arctic sea ice, *Geophys. Res. Lett.*, *39*, L08501, doi:10.1029/2012GL051432.
Perovich, D. K., T. C. Grenfell, B. Light, and P. V. Hobbs (2002), Seasonal evolution of the albedo of multiyear Arctic sea ice, *J. Geophys. Res.*, *107*(C10), 8044, doi:10.1029/2000JC000438.
Perovich, D. K., S. V. Nghiem, T. Markus, and A. Schweiger (2007), Seasonal evolution and interannual variability of the local solar energy absorbed by the Arctic sea ice-ocean system, *J. Gerophys. Res.*, *112*, C03005, doi:10.1029/2006JC003558.
Perovich, D. K., J. A. Richter-Menge, K. F. Jones, and B. Light (2008), Sunlight, water, and ice: Extreme Arctic sea ice melt during the summer of 2007, *Geophys. Res. Lett.*, *35*, L11501, doi:10.1029/2008GL034007.
Perovich, D. K., K. F. Jones, B. Light, H. Eicken, T. Markus, J. Stroeve, and R. Lindsay (2011a), Solar partitioning in a changing Arctic sea-ice cover, *Ann. Glaciol.*, *52*(57), 192–196.
Perovich, D. K., J. A. Richter-Menge, K. F. Jones, B. Light, B. C. Elder, C. Polashenski, D. Laroche, T. Markus, and R. Lindsay (2011b), Arctic sea-ice melt in 2008 and the role of solar heating, *Ann. Glaciol.*, *52*(57), 355–359.
Perovich, D. K., S. Gerland, S. Hendricks, W. Meier, M. Nicolaus, J. Richter-Menge, and M. Tschudi (2013), Sea ice: [in Arctic Report Card 2013]. [Available at http://www.arctic.noaa.gov/reportcard.]
Perovich, D. K., J. Richter-Menge, C. Polashenski, B. Elder, T. Arbetter, and O. Brennick (2014a), Sea ice mass balance observations from the North Pole Environmental Observatory, *Geophys. Res. Lett.*, *41*, 2019–2025, doi:10.1002/2014GL059356.
Perovich, D. K., S. Gerland, S. Hendricks, W. Meier, M. Nicolaus, and M. Tschudi (2014b), Sea ice: [in Arctic Report Card 2014]. [Available at http://www.arctic.noaa.gov/reportcard.]
Perovich, D. K., J. Richter-Menge, B. Elder, T. Arbetter, K. Claffey, and C. Polashenski (2014c), Observing and understanding climate changes: Monitoring the mass balance, motion, and thickness of Arctic sea ice. [Available at http://imb.erdc.dren.mil.]
Persson, P. O. G., C. W. Fairall, E. Andreas, P. Guest, and D. K. Perovich (2002), Measurements near the atmospheric surface flux group tower at SHEBA: Near-surface conditions and surface energy budget, *J. Geophys. Res.*, *107*(C10), 8045, doi:10.1029/2000JC000705.
Polashenski, C., D. Perovich, and Z. Courville (2012), The mechanisms of sea ice melt pond formation and evolution, *J. Geophys. Res.*, *117*, C01001, doi:10.1029/2011JC007231.
Polyakov, I. V., et al. (2010), Arctic ocean warming contributes to reduced polar ice cap, *J. Phys. Oceanogr.*, *40*, 2743–2756.

Renner, A. H. H., S. Gerland, C. Haas, G. Spreen, J. F. Beckers, E. Hansen, M. Nicolaus, and H. Goodwin (2014), Evidence of Arctic sea ice thinning from direct observations, *Geophys. Res. Lett.*, *41*, 5029–5036, doi:10.1002/2014GL060369.

Richter-Menge, J., D. K. Perovich, B. C. Elder, K. Claffey, I. Rigor, and M. Ortmeyer (2006), Ice mass balance buoys: A tool for measuring and attributing changes in the thickness of the Arctic sea ice cover, *Ann. Glaciol.*, *44*, 205–210.

Saha, S., et al. (2014), The NCEP climate forecast system version 2, *J. Clim.*, *27*, 2185–2208.

Schröder, D., D. L. Feltham, D. Flocco, and M. Tsamados (2014), September Arctic sea-ice minimum predicted by spring melt-pond fraction, *Nature Clim. Change*, *4*, 353–357, doi:10.1038/NCLIMATE2203.

Simmonds, I., and I. Rudeva (2012), The great Arctic cyclone of August 2012, *Geophys. Res. Lett.*, *39*, L23709, doi:10.1029/2012GL054259.

Smith, D. M. (1998), Recent increase in the length of the melt season of perennial Arctic sea ice, *Geophys. Res. Lett.*, *25*, 655–658, doi:10.1029/98GL00251.

Steel, M., W. Ermold, and J. Zhang (2008), Arctic Ocean surface warming trends over the past 100 years, *Geophys. Res. Lett.*, *35*, L02614, doi:10.1029/2007GL031651.

Stroeve, J. C., T. Markus, L. Boisvert, J. Miller, and A. Barret (2014), Changes in Arctic melt season and implications for sea ice loss, *Geophys. Res. Lett.*, *41*, 1216–1225, doi:10.1002/2013GL058951.

Wang, C., M. A. Granskog, S. Gerland, S. R. Hudson, D. K. Perovich, M. Nicolaus, T. I. Karlsen, K. Fossan, and M. Bratrein (2014), Autonomous observations of solar energy partitioning in first-year sea ice in the Arctic Basin, *J. Geophys. Res. Oceans*, *119*, 2066–2080, doi:10.1002/2013JC009459.

Wang, L., C. Derksen, R. Brown, and T. Markus (2013), Recent changes in pan-Arctic melt onset from satellite passive microwave measurements, *Geophys. Res. Lett.*, *40*, 522–528, doi:10.1002/grl.50098.

Wiscome, W. J., and S. G. Warren (1980), A model for the spectral albedo of snow. I: Pure snow, *J. Atmos. Sci.*, *37*, 2712–2733.

Zhang, J., R. Lindsay, A. Schweiger, and M. Steele (2013), The impact of an intense summer cyclone on 2012 Arctic sea ice retreat, *Geophys. Res. Lett.*, *40*, 720–726, doi:10.1002/grl.50190.